Reflected Shock Tube and Theoretical Studies of High-Temperature Rate Constants for OH + $CF_3H \leftrightarrows CF_3 + H_2O$ and CF_3 + OH → Products†

N. K. Srinivasan, M.-C. Su,‡ J. V. Michael,* S. J. Klippenstein, and L. B. Harding

Chemistry Division, Argonne National Laboratory, Argonne, Illinois 60439

Received: January 24, 2007; In Final Form: March 13, 2007

The reflected shock tube technique with multipass absorption spectrometric detection of OH radicals at 308 nm, using either 36 or 60 optical passes corresponding to total path lengths of 3.25 or 5.25 m, respectively, has been used to study the bimolecular reactions, OH + $CF_3H \rightarrow CF_3 + H_2O$ (1) and $CF_3 + H_2O \rightarrow$ OH + CF_3H (−1), between 995 and 1663 K. During the course of the study, estimates of rate constants for CF_3 + OH → products (2) could also be determined. Experiments on reaction −1 were transformed through equilibrium constants to k_1, giving the Arrhenius expression $k_1 = (9.7 \pm 2.1) \times 10^{-12} \exp(-4398 \pm 275K/T)$ cm^3 molecule^{-1} s^{-1}. Over the temperature range, 1318−1663 K, the results for reaction 2 were constant at $k_2 = (1.5 \pm 0.4) \times 10^{-11}$ cm^3 molecule^{-1} s^{-1}. Reactions 1 and −1 were also studied with variational transition state theory (VTST) employing QCISD(T) properties for the transition state. These a priori VTST predictions were in good agreement with the present experimental results but were too low at the lower temperatures of earlier experiments, suggesting that either the barrier height was overestimated by about 1.3 kcal/mol or that the effect of tunneling was greatly underestimated. The present experimental results have been combined with the most accurate earlier studies to derive an evaluation over the extended temperature range of 252−1663 K. The three parameter expression $k_1 = 2.08 \times 10^{-17} T^{1.5513} \exp(-1848\ K/T)$ cm^3 molecule^{-1} s^{-1} describes the rate behavior over this temperature range. Alternatively, the expression $k_{1,th} = 1.78 \times 10^{-23} T^{3.406} \exp(-837\ K/T)$ cm^3 molecule^{-1} s^{-1} obtained from empirically adjusted VTST calculations over the 250−2250 K range agrees with the experimental evaluation to within a factor of 1.6. Reaction 2 was also studied with direct CASPT2 variable reaction coordinate transition state theory. The resulting predictions for the capture rate are found to be in good agreement with the mean of the experimental results and can be represented by the expression $k_{2,th} = 2.42 \times 10^{-11} T^{-0.0650} \exp(134\ K/T)$ cm^3 molecule^{-1} s^{-1} over the 200−2500 K temperature range. The products of this reaction are predicted to be CF_2O + HF.

Introduction

The reactions of CF_3 radicals play an important role in the flame retardant properties of halons, particularly CF_3Br.[1−3] Because of their ozone depletion potentials in the atmosphere, these molecules have been banned, and replacement molecules have been proposed.[4,5] Although mechanisms for the destruction of the halons, CF_3Cl and CF_3Br, and also of CF_3H and CF_3I in flames, have been proposed,[6−9] there are many reaction rate constants that are still estimated and not experimentally justified.[10] This shortcoming motivated work from this laboratory on the thermal decompositions for three of these molecules.[11−13] CF_3H is a byproduct formed in the production of the important refrigerant, HCFC-22 ($CHClF_2$); however, CF_3H as an atmospheric greenhouse gas has a global warming potential of 11 700, making it necessary to remove this molecule by incineration from the HCFC-22 production process. The high-temperature reactions involved in incineration are not well-known, and this prompted earlier studies from this laboratory on the bimolecular destruction rates of CF_3H by H and its reverse, $CF_3 + H_2$.[14] It is this prior interest that has motivated the present study on the reversible reactions

$$OH + CF_3H \rightarrow CF_3 + H_2O \quad (1)$$

$$CF_3 + H_2O \rightarrow OH + CF_3H \quad (-1)$$

We earlier described a long absorption path multipass optical system for OH radical detection in the reflected shock regime[15] and used it to measure other high-temperature rate constants.[16−18] The method involves measuring absolute [OH] temporal profiles and fitting a detailed mechanism to simulate the results. During the course of the work, we were additionally able to derive rate constant values for the secondary reaction

$$CF_3 + OH \rightarrow \text{products} \quad (2)$$

As a supplement to these experimental studies, we have also performed ab initio based variational transition state theory (TST) studies of the CF_3H + OH and CF_3 + OH reactions. The former reaction has been the subject of a few prior theoretical kinetics studies.[19−22] The present work proceeds beyond these studies by (i) implementing higher level quantum chemical estimates, (ii) considering the effects of anharmonicities on the transition state partition functions, (iii) including variational treatments, and (iv) considering tunneling through the vibrationally adiabatic ground state potential.

† Part of the special issue "M. C. Lin Festschrift".

* Corresponding author. Phone: (630) 252-3171. Fax: (630) 252-4470. E-mail: jmichael@anl.gov.

‡ Special Term Appointment, Argonne. Permanent address: Department of Chemistry, Sonoma State University, 1801 E. Cotati Ave., Rohnert Park, CA 94928.

10.1021/jp0706228 CCC: $37.00
Published on Web 05/16/2007

The CF_3 + OH reaction does not appear to have been the subject of any prior theoretical kinetics study. Here, we first consider the potential energy surface for this reaction with G3//B3LYP[23] calculations. This analysis predicts that the products are CF_2O + HF and, furthermore, that the reaction rate should be governed by the addition rate. To calculate this addition rate, we implement our direct CASPT2 variable reaction coordinate transition state theory approach.[24,25]

Experimental Procedures

The present experiments were performed with the shock tube technique using OH radical electronic absorption detection. The method and the apparatus currently being used have been previously described,[26,27] and only a brief description of the experiment will be presented here.

The shock tube was constructed from 304 stainless steel in three sections. The first 10.2 cm o.d. cylindrical section was separated from the He driver chamber by a 4 mil unscored 1100-H18 aluminum diaphragm. A 0.25 m transition section then connected the first and third sections. The third section was of a rounded corner (radius, 1.71 cm) square design and was fabricated from flat stock (3 mm) with a mirror finish. Two flat fused silica windows (3.81 cm) with broadband antireflection (BB AR) coatings for UV light were mounted on the tube across from one another at a distance of 6 cm from the end plate. The path length between the windows was 8.745 cm. The incident shock velocity was measured with eight fast pressure transducers (PCB Piezotronics, Inc., Model 113A21) mounted along the third portion of the shock tube, and the temperature and density in the reflected shock wave regime were calculated from this velocity and included corrections for boundary layer perturbations.[28−30] The tube was routinely pumped between experiments to $<10^{-8}$ Torr by an Edwards Vacuum Products Model CR100P packaged pumping system. A 4094C Nicolet digital oscilloscope was used to record the velocities, and an LC334A LeCroy digital oscilloscope was used to record the absorption signals.

The optical configuration consisted of an OH resonance lamp,[15,16] multipass reflectors, an interference filter at 308 nm, and a photomultiplier tube (1P28) all mounted external to the shock tube as described previously.[15−17,31] With this new configuration, we were able to obtain multiple passes, thereby amplifying the measured absorbances.

Gases. High-purity He (99.995%), used as the driver gas, was from AGA Gases. Scientific grade Kr (99.999%), the diluent gas in reactant mixtures, was from Spectra Gases, Inc. The ~10 ppm impurities (N_2− 2 ppm, O_2− 0.5 ppm, Ar− 2 ppm, CO_2− 0.5 ppm, H_2− 0.5 ppm, CH_4− 0.5 ppm, H_2O− 0.5 ppm, Xe− 5 ppm, and CF_4− 0.5 ppm) were all either inert or in sufficiently low concentrations so as to not perturb the OH radical profiles. Distilled water, evaporated at 1 atm into ultrahigh-purity grade Ar (99.999%) from AGA Gases, was used at ~25 Torr in the resonance lamp. Analytical grade CF_3H (99% from AGA Gases) and CF_3I (97% from SynQuest Laboratories, Inc.) were further purified by bulb-to-bulb distillations with the middle thirds being retained. Triple distilled H_2O was also purified by bulb-to-bulb vacuum distillation retaining the middle third. T-HYDRO *tert*-butylhyroperoxide (70% *t*BH by weight water solution; i.e., 32 mol % *t*BH and 68 mol % H_2O) was obtained from the Aldrich Chemical Co. In the *t*BH experiments, 0.45 cm^3 of the solution was completely evaporated into the glass vacuum line, and all mixtures were then manometrically made from the evaporated sample.

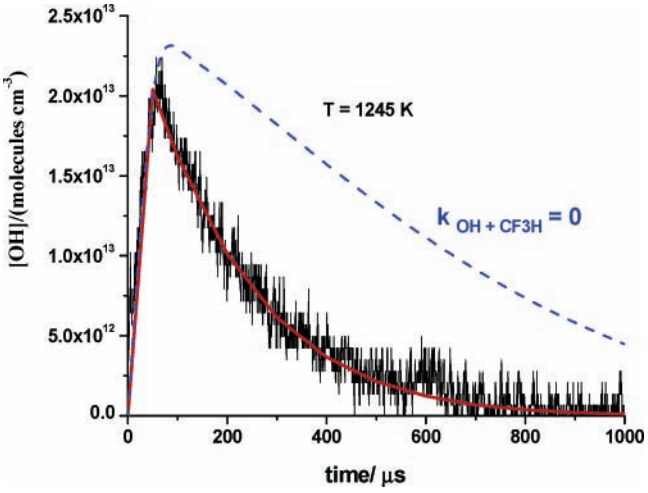

Figure 1. Sample temporal profile of OH absorption. Solid line: fit with full reaction mechanism. Dashed line: simulation with $k_1 = 0$. $P_1 = 10.99$ Torr, $M_s = 2.240$, $T_5 = 1245$ K, $\rho_5 = 1.932 \times 10^{18}$ molecules cm^{-3}, $[TBH]_0 = 2.500 \times 10^{13}$ molecules cm^{-3}, $[H_2O]_0 = 6.016 \times 10^{13}$, and $[CF_3H]_0 = 1.208 \times 10^{16}$ molecules cm^{-3}.

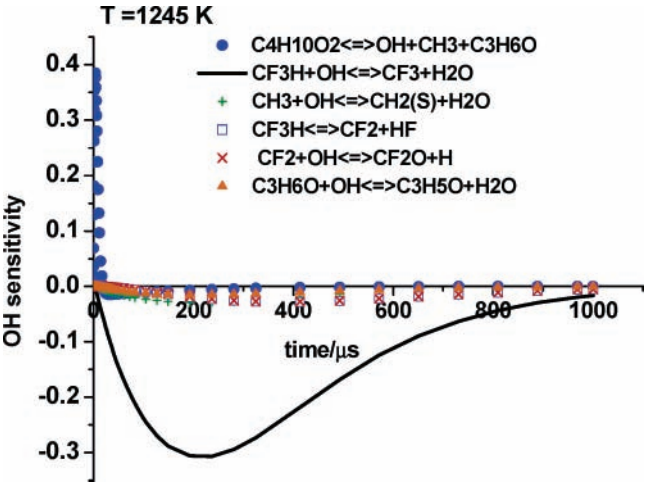

Figure 2. OH radical sensitivity analysis for the 1245 K profile shown in Figure 1 using the full reaction mechanism scheme and the final fitted value of $k_1 = 3.00 \times 10^{-13}$ cm^3 $molecule^{-1}$ s^{-1}. The six most sensitive reactions are shown as an inset.

Results

Experiments. OH + CF_3H → CF_3 + H_2O. OH radicals were produced from the thermal decomposition of *t*BH. The experiments were performed with ~44 ppm *t*BH solution and 6250 ppm CF_3H between 995 and 1316 K. The lower temperature limit was dictated by a low signal-to-noise ratio while the thermal decomposition of *t*BH in the incident shock wave at $T > 1300$ K dictated the upper temperature limit. The temporal concentration decrease of OH was determined from measured absorbance $(ABS)_t = \ln[I_0/I_t] = [OH]_t l \sigma_{OH}$, through an earlier determination[17] of the absorption cross-section at 308 nm ($\sigma_{OH} = (4.516-1.18 \times 10^{-3}\ T) \times 10^{-17}$ cm^2 $molecule^{-1}$). We used 36 optical passes (i.e., path length = 3.15 m). The pressure range was 163−271 Torr. A typical result at 1245 K is shown in Figure 1 along with a simulation using the mechanism of Table 1 where k_1 is the only rate constant that was varied. Figure 2 shows a sensitivity analysis corresponding to Figure 1, and it is clear that the profile is dominated by reaction 1. The rate constant values from 12 profiles are listed in Table 2 along with the conditions for each experiment. In

TABLE 1: Mechanism for Fitting [OH] Profiles for OH + $CF_3H \leftrightarrows CF_3 + H_2O$

	reaction	rate[a]	ref
1	$CF_3I + Kr \rightarrow CF_3 + I + Kr$	$k_1 = 2.86 \times 10^{-9} \exp(-15943\ K/T)$	12
2	$H + O_2 \rightarrow OH + O$	$k_2 = 1.62 \times 10^{-10} \exp(-7474\ K/T)$	32
3	$OH + O \rightarrow O_2 + H$	$k_3 = 5.42 \times 10^{-13}\ T^{0.375} \exp(950\ K/T)$	26, 33, 34
4	$O + H_2 \rightarrow OH + H$	$k_4 = 8.44 \times 10^{-20}\ T^{2.67} \exp(-3167\ K/T)$	26
5	$OH + H \rightarrow H_2 + O$	$k_5 = 3.78 \times 10^{-20}\ T^{2.67} \exp(-2393\ K/T)$	26, 33, 34
6	$OH + H_2 \rightarrow H_2O + H$	$k_6 = 3.56 \times 10^{-16}\ T^{1.52} \exp(-1736\ K/T)$	35
7	$H_2O + H \rightarrow OH + H_2$	$k_7 = 1.56 \times 10^{-15}\ T^{1.52} \exp(-9083\ K/T)$	26, 33, 34
8	$OH + OH \rightarrow O + H_2O$	$k_8 = 7.19 \times 10^{-21}\ T^{2.7} \exp(917\ K/T)$	26, 33, 34, 36
9	$O + H_2O \rightarrow OH + OH$	$k_9 = 7.48 \times 10^{-20}\ T^{2.7} \exp(-7323\ K/T)$	26, 33, 34
10	$HCO + Kr \rightarrow H + CO + Kr$	$k_{10} = 6.00 \times 10^{-11} \exp(-7722\ K/T)$	37
11	$HO_2 + Kr \rightarrow H + O_2 + Kr$	$k_{11} = 7.614 \times 10^{-10} \exp(-22520\ K/T)$	38
12	$H_2CO + OH \rightarrow H_2O + HCO$	$k_{12} = 5.69 \times 10^{-15}\ T^{1.18} \exp(225\ K/T)$	39
13	$I + O_2 \rightarrow IO + O$	$k_{13} = 7 \times 10^{-11} \exp(-30977\ K/T)$	40
14	$CH_3 + CH_3 \rightarrow C_2H_6$	$k_{14} = (\rho, T)$	41
15	$CH_3 + CH_3 \rightarrow C_2H_4 + 2H$	$k_{15} = 5.26 \times 10^{-11} \exp(-7392\ K/T)$	42
16	$CH_3 + O \rightarrow H_2CO + H$	$k_{16} = 1.148 \times 10^{-10}$	43, 44
17	$CH_3 + OH \rightarrow {}^1CH_2 + H_2O$	$k_{17} = 1.81 \times 10^{-14}\ T - 9.13 \times 10^{-12}$	45
18	$O + C_2H_6 \rightarrow OH + H + C_2H_4$	$k_{18} = 1.87 \times 10^{-10} \exp(-3950\ K/T)$	46
19	$OH + C_2H_4 \rightarrow H_2O + H + C_2H_2$	$k_{19} = 3.35 \times 10^{-11} \exp(-2990\ K/T)$	47
20	${}^1CH_2 + Kr \rightarrow {}^3CH_2 + Kr$	$k_{20} = 4.0 \times 10^{-14}\ T^{0.93}$	48, 49
21	$OH + {}^3CH_2 \rightarrow CH_2O + H$	$k_{21} = 1.110 \times 10^{-10}\ T^{0.0166} \exp(-9.1\ K/T)$	50
22	${}^3CH_2 + {}^3CH_2 \rightarrow C_2H_2 + 2H$	$k_{22} = 2.395 \times 10^{-10}\ T^{0.0254} \exp(-17.1\ K/T)$	50
23	${}^3CH_2 + CH_3 \rightarrow C_2H_4 + H$	$k_{23} = 3.789 \times 10^{-10}\ T^{-0.1317} \exp(-8.2\ K/T)$	50
24	${}^3CH_2 + H \rightarrow CH + H_2$	$k_{24} = 2 \times 10^{-10}$	50
25	$HO_2 + OH \rightarrow H_2O + O_2$	$k_{25} = 2.35 \times 10^{-10}\ T^{-0.21} \exp(56\ K/T)$	51
26	$CH_3 + O \rightarrow H_2 + CO + H$	$k_{26} = 2.52 \times 10^{-11}$	43, 44
27	$C_4H_{10}O_2 \rightarrow OH + CH_3 + (CH_3)_2CO$	$k_{27} = 2.5 \times 10^{15} \exp(-21649\ K/T)$	52
28	$CF_3 + OH \rightarrow CF_2O + HF$	k_{28} = see text	
29	$CF_3H + O \rightarrow CF_3 + OH$	$k_{29} = 3.69 \times 10^{-18}\ T^{2.36} \exp(-7294\ K/T)$	53
30	$CF_3H + OH \rightarrow CF_3 + H_2O$	k_{30} = see text	
31	$CF_3 + H_2O \rightarrow CF_3H + OH$	$k_{31} = k_{30}\,(4.125 \times 10^{-12}\ T^3 - 3.29 \times 10^{-9} T^2 - 1.55 \times 10^{-6}\ T + 1.381 \times 10^{-3})$	
32	$CF_3 + CH_3 \rightarrow C_2H_2F_2 + HF$	$k_{32} = 2.1 \times 10^{-11}$	54
33	$CF_3H + Kr \rightarrow CF_2 + HF$	k_{33} is interpolated from Figure 5 in ref 55	55
34	$CF_2 + OH \rightarrow CF_2O + H$	$k_{34} = 2 \times 10^{-11}$	54
35	$CF_3 + Kr \rightarrow CF_2 + F$	$k_{35} = 4.46 \times 10^{-8} \exp(-34836\ K/T)$	54
36	$F + H_2O \rightarrow OH + HF$	$k_{36} = 1.45 \times 10^{-11}$	56
37	$OH + (CH_3)_2CO \rightarrow H_2O + CH_2COCH_3$	$k_{37} = 4.90 \times 10^{-11} \exp(-2297\ K/T)$	57
38	$OH + C_2H_6 \rightarrow H_2O + H + C_2H_4$	$k_{38} = 2.68 \times 10^{-18}\ T^{2.22} \exp(-373\ K/T)$	58

[a] All rate constants are in cm^3 $molecule^{-1}$ s^{-1} except for *reaction 27*, which is in s^{-1}.

all cases, the dominant rate process dictating the profiles is reaction 1. Hence, the derived rate constants are nearly direct (i.e., almost pseudo-first-order). The fourth column in Table 2 shows the initial fraction of *t*BH that was necessary to fit the profiles, and the average value is ~30 mol %. The solution from which the mixtures were prepared was 32 mol %, showing that little if any *t*BH was lost either in the glass vacuum line storage or in the transfer into the shock tube.

$CF_3 + H_2O \rightarrow OH + CF_3H$. Sixteen experiments on reaction −1 were carried out between 1318 and 1663 K over the pressure range of 283−398 Torr, using 73−77 ppm CF_3I and 2.6−4.8% H_2O. We used 60 optical passes, giving a total path length of 5.25 m. The formation of OH was measured, and the profile fits were also determined using the mechanism of Table 1. Figure 3 shows simulations for two experiments at 1663 and 1368 K, respectively. The corresponding sensitivity analysis for the higher temperature experiment is presented in Figure 4. In this case, only three reactions contribute to OH sensitivity; however, CF_3 dissociation (reaction 35 in Table 1) becomes increasingly important only when the temperature is high. This dissociation limits the upper temperature range over which k_{-1} can be determined. It becomes negligible as *T* decreases. Hence, over most of the temperature range, the simulations involve the simultaneous adjustment of two reactions, namely, reactions −1 and 2. Since both rate constants exhibit similar sensitivities, only with opposite signs to each other, one would expect that uncertainties of ±25% in k_{-1} would be approximately compensated by ±25% variations in k_2; however, as seen in Figure 3, such variations result in worse fits. The accuracy of the fits for the entire data set is estimated to be approximately ±20%. Hence, the mutual values for both k_{-1} and k_2, presented in Table 2, represent the best fits to the data and easily reproduce the experiments to within approximately ±5%.

Theory. OH + $CF_3H \rightarrow CF_3 + H_2O$. The rovibrational properties of the stationary points for the CF_3H + OH abstraction reaction were determined from quadratic configuration interaction calculations with perturbative inclusion of the triples contribution [QCISD(T)][59] employing Dunning's augmented correlation-consistent polarized valence double-ζ (adz) basis set.[60] Complete basis set energies, QCISD(T)/CBS, were estimated by extrapolation[61−63] of QCISD(T) calculations with the related triple and quadruple-ζ basis sets at these QCISD(T)/adz optimized geometries. Notably, the QCISD(T)/CBS zero-point corrected abstraction barrier of 6.33 kcal/mol is only 0.1 kcal/mol lower than that obtained with the adz basis set. This similarity suggests that the imaginary frequency obtained from the QCISD(T)/adz calculations should be close to the basis set limit. Restricted spin wavefunctions were employed in these calculations.

These QCISD(T)/CBS energies and QCISD(T)/adz vibrational frequencies were implemented in standard rigid-rotor harmonic oscillator (RRHO) based TST calculations of the abstraction rate. Corrections for variational, anharmonic, and tunneling effects were appended to these RRHO fixed TST

TABLE 2: High-Temperature Rate Data

P_1 (Torr)	M_s[a]	ρ_5 (10^{18} cm^{-3})[b]	T_5 (K)[b]	$[TBH]_0/[TBH + H_2O]_0$	k_1[c]
		OH + $CF_3H \rightarrow CF_3 + H_2O$			
$X_{CF_3H} = 6.250 \times 10^{-3}$		$X_{TBH+H_2O} = 4.407 \times 10^{-5}$			
10.96	2.210	1.897	1217	0.30	2.50(−13)[d]
10.99	2.240	1.932	1245	0.29	3.00(−13)
10.89	2.312	1.990	1316	0.28	3.10(−13)
10.98	2.187	1.869	1198	0.28	2.40(−13)
10.92	2.158	1.835	1166	0.28	2.15(−13)
10.90	2.179	1.847	1190	0.27	2.40(−13)
10.88	2.134	1.797	1147	0.30	2.40(−13)
10.88	2.121	1.782	1134	0.30	2.30(−13)
10.88	2.093	1.747	1112	0.29	1.90(−13)
10.97	2.058	1.722	1080	0.28	1.55(−13)
10.97	2.031	1.685	1058	0.27	1.45(−13)
10.90	1.957	1.586	995	0.27	1.30(−13)
		$CF_3 + H_2O \rightarrow$ OH + CF_3H and CF_3 + OH → CF_2O + HF			
$X_{CF_3I} = 7.715 \times 10^{-5}$		$X_{H_2O} = 4.615 \times 10^{-2}$		k_{-1}	k_2
10.88	2.514	2.227	1502	4.12(−15)	1.60(−11)
10.98	2.557	2.296	1544	4.88(−15)	1.80(−11)
10.94	2.489	2.216	1476	3.16(−15)	1.63(−11)
10.95	2.518	2.246	1507	3.49(−15)	1.60(−11)
10.91	2.514	2.234	1503	3.50(−15)	1.90(−11)
$X_{CF_3I} = 7.368 \times 10^{-5}$		$X_{H_2O} = 4.800 \times 10^{-2}$			
10.97	2.406	2.153	1383	1.60(−15)	1.00(−11)
10.88	2.387	2.108	1368	1.16(−15)	1.00(−11)
10.96	2.337	2.073	1318	7.92(−16)	9.50(−12)
10.96	2.355	2.091	1335	9.44(−16)	1.10(−11)
10.99	2.451	2.193	1433	2.01(−15)	1.45(−11)
10.96	2.581	2.320	1567	3.81(−15)	2.00(−11)
$X_{CF_3I} = 7.298 \times 10^{-5}$		$X_{H_2O} = 2.593 \times 10^{-2}$			
10.94	2.451	2.143	1455	2.42(−15)	1.00(−11)
10.96	2.538	2.233	1544	3.18(−15)	1.50(−11)
10.95	2.639	2.311	1663	6.01(−15)	2.00(−11)
10.98	2.600	2.292	1614	3.91(−15)	2.00(−11)
10.97	2.573	2.267	1584	3.31(−15)	1.80(−11)

[a] Error in measuring the Mach number, M_s, is typically 0.5−1.0% at the one standard deviation level. [b] Quantities with the subscript 5 refer to the thermodynamic state of the gas in the reflected shock region. [c] Rate constants in units cm^3 molecule^{-1} s^{-1}. [d] Parentheses denotes the power of 10.

results. The OH partition function for the reactants was evaluated via a direct sum over the rovibronically coupled levels of the $^2\Pi_{1/2}$ and $^2\Pi_{3/2}$ states. For the transition state, we assume that the spin−orbit coupling is negligible and consider only the lowest electronic state.

The rovibrational properties of the saddle point were also studied with B3LYP[64] density functional calculations employing the 6-311++G(d,p) basis set and unrestricted spin wavefunctions.[65] Although the saddle point geometry does differ somewhat from the QCISD(T)/adz geometry (the CH and OH separations for the abstracting H atom are 0.018 and 0.030 Å smaller and greater, respectively), the QCISD(T)/adz barrier height at the B3LYP/6-311++G(d,p) geometry is within 0.02 kcal/mol of its fully optimized value. With two exceptions, the vibrational frequencies from the B3LYP calculations are reasonably similar to those from the QCISD(T) ones. The two exceptions are the imaginary frequency, with QCISD(T) and B3LYP values of −2028 and −1207, respectively, and the HO••CH torsional frequency, with values of 109 and −39 for the cis saddlepoint. In reality, the torsional mode has a very flat potential, with a QCISD(T)/CBS estimated barrier of about 0.07 kcal/mol. Thus, this mode was treated as a free rotor in the TST kinetics evaluations. For reference purposes, the geometries and vibrational frequencies from both B3LYP/6-311++G(d,p) and QCISD(T)/adz evaluations are provided in the Supporting Information.

In addition to the torsion mode, two other modes, the in- and out-of-plane OHC bends, have vibrational frequencies below 200 cm^{-1}. For such low vibrational frequencies, anharmonic effects may be significant. Here, we have implemented one-dimensional semiclassical treatments of the anharmonic effects for these modes in analogy with our recent treatment of the methyl umbrella mode.[66] The importance of the anharmonicity in these modes for OH abstraction reactions was recently noted by Seta and co-workers[67] in their study of the reactions of benzene and toluene with OH, and our treatment is closely analogous to theirs. The one-dimensional potential for these evaluations is obtained from QCISD(T)/adz evaluations.

The minimum energy path was followed in mass weighted Cartesian coordinates with the B3LYP/6-311++G(d,p) method. Then, along this pathway, energies were evaluated at the QCISD(T)/adz level, and projected vibrational frequencies were obtained with the B3LYP/6-311++G(d,p) method. The latter two evaluations provided the basis for the evaluation of the variational and tunneling corrections. In particular, variational corrections were obtained from the minimization of E/J resolved RRHO evaluations of the number of states employing the QCISD(T)/adz energies and the B3LYP/6-311++G(d,p) projected vibrational frequencies. Tunneling corrections were obtained from semiclassical evaluations of the transmission probability through the vibrationally adiabatic ground state, following the prescription of Garrett and Truhlar.[68] The vibra-

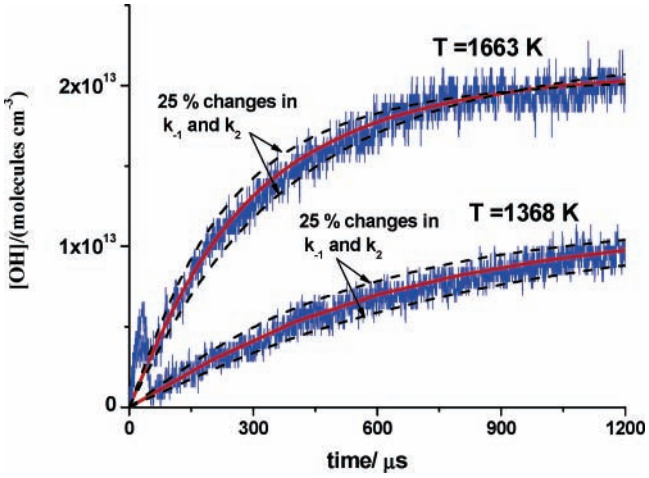

Figure 3. Two temporal profiles of OH absorption measured at two different temperatures. Solid lines: fits with full reaction mechanism listed in Table 1. Dashed lines: simulations with ±25% changes in k_{-1} and k_2. The conditions for the high-temperature profile are $P_1 = 10.95$ Torr, $M_s = 2.639$, $T_5 = 1663$ K, $\rho_5 = 2.311 \times 10^{18}$ molecules cm^{-3}, $[CF_3I]_0 = 1.686 \times 10^{14}$ molecules cm^{-3}, and $[H_2O]_0 = 5.992 \times 10^{16}$ molecules cm^{-3}. Conditions for the low-temperature profile are $P_1 = 10.88$ Torr, $M_s = 2.387$, $T_5 = 1368$ K, $\rho_5 = 2.108 \times 10^{18}$ molecules cm^{-3}, $[CF_3I]_0 = 1.554 \times 10^{14}$ molecules cm^{-3}, and $[H_2O]_0 = 1.012 \times 10^{17}$ molecules cm^{-3}.

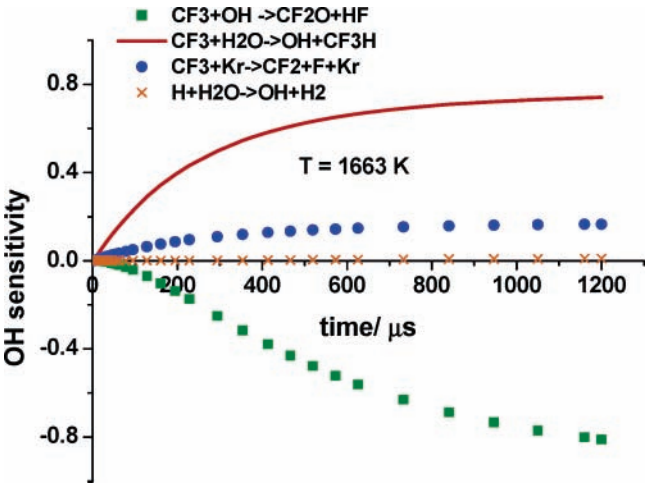

Figure 4. OH radical sensitivity analysis for the 1663 K profile shown in Figure 3 using the full reaction mechanism scheme and the final fitted values of $k_{-1} = 6.01 \times 10^{-15}$ and $k_2 = 2 \times 10^{-11}$ cm^3 molecule^{-1} s^{-1}. The four most sensitive reactions are shown as an inset.

tionally adiabatic ground state (VAG) potential was taken as the sum of the QCISD(T)/adz//B3LYP/6-311++G(d,p) energies and the B3LYP/6-311++G(d,p) zero-point energy. For comparison purposes, the transmission probability was also evaluated for an asymmetric Eckart potential.

A plot of the B3LYP/6-311++G(d,p), QCISD(T)/adz//B3LYP/6-311+G(d,p), and VAG minimum energy path potentials for the trans abstraction pathway is provided in Figure 5. For each of these plots, the reactants are taken as the zero of energy. Notably, the curvature of these potentials is significantly different, implying quite different transmission probabilities, as expounded on in the recent study of the OH + CH_xF_{4-x} abstraction reactions by Schwartz et al.[21] The VAG potential, which is the flattest of the three, provides the more fundamentally meaningful potential. However, a quantitatively accurate consideration of tunneling should also consider alternative

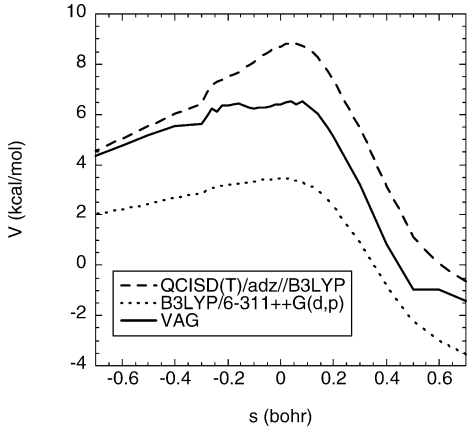

Figure 5. Plot of the minimum energy path potentials for the CF_3H + OH reaction.

tunneling paths such as the Marcus−Coltrin corner cutting path.[69] Such considerations are likely to yield an increased transmission probability. Truhlar and co-workers have provided various prescriptions for considering such paths.[70−72] However, such calculations are considerably more difficult and were deemed beyond the scope of this work, particularly since here we are primarily interested in the high-temperature regime where tunneling is unlikely to be significant.

The Q1 diagnostic for the QCISD(T)/qz//QCISD(T)/adz calculations, which provides some measure of the extent of multireference character to the wavefunction,[73,74] was 0.026 at the saddle point. This value is just large enough to cause some minor concern regarding the suitability of such a single reference based method. For this reason, equivalent calculations were performed for the closely related H_2 + OH abstraction where other higher level calculations can also be performed. For the latter reaction, the QCISD(T) calculations were found to be in good agreement with internally contracted Davidson-corrected[75] multireference single and double excitation configuration interaction (MRCI) calculations. In particular, for a full valence active space and the adz basis set, the barrier heights were within 0.07 kcal/mol, and the geometries were within 0.001 Å. Furthermore, full CI calculations employing the 6-31G* basis set (at the QCISD(T)/adz optimized geometries) yielded a barrier height that also agreed with related QCISD(T)/6-31G* calculations to within 0.07 kcal/mol. Interestingly, the QCISD(T)/CBS//QCISD(T)/adz potential barrier height of 5.22 kcal/mol (before zero-point correction) also closely matches the value of 5.40 kcal/mol, which Yang et al.[76] found yields quantitative agreement with experiment in their wavepacket study of the H_2 + OH reaction. Notably, for this reaction, the Q1 diagnostic at the saddle point, 0.040, is even greater than for the CF_3H + OH reaction.

The CH_4 + OH abstraction is another small and closely related system, and it has also been widely studied. Unfortunately, in this case, we are unable to do full valence MRCI calculations. More limited three electron and three orbital active space MRCI/adz and CASPT2/adz calculations yield barrier heights that are 1.52 kcal/mol above and 0.84 kcal/mol below the QCISD(T)/adz barrier height, respectively. For this reaction, the Q1 diagnostic is 0.032. A fairly recent variational transiton state theory study[77] obtains good agreement with experiment for a zero-point corrected barrier of 4.9 kcal/mol, which matches closely the present QCISD(T)/CBS//QCISD(T)/adz value of 4.73 kcal/mol.

We have also examined the dependence of the vibrational frequencies on the basis set for the CH_4 + OH and H_2 + OH

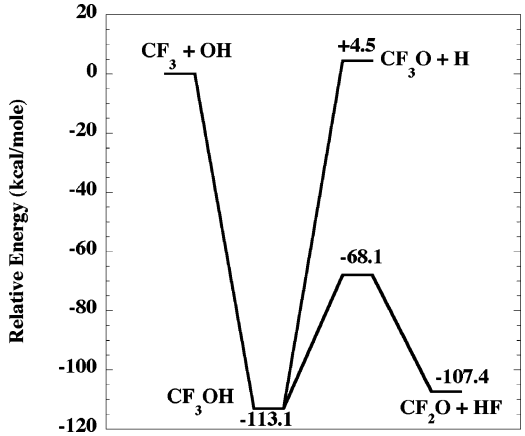

Figure 6. Schematic plot of the G3//B3LYP potential energy surface for the CF_3 + OH reaction at 0 K.

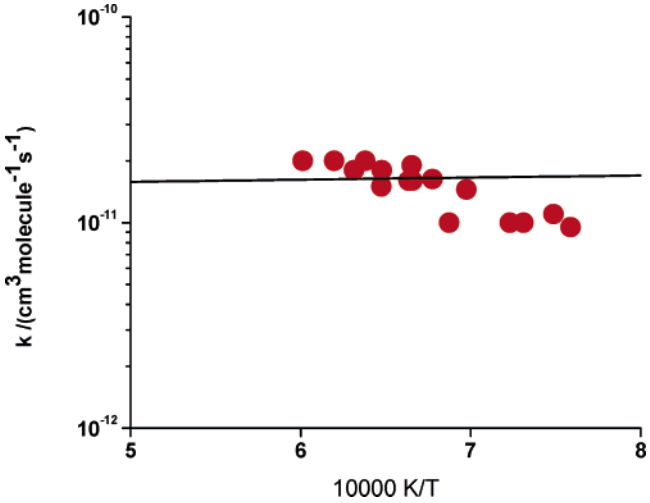

Figure 7. Arrhenius plot of the data for k_2 from Table 2. Red circles: present work (1318−1663 K). Thick solid line: theoretical calculation, eq 3.

systems. QCISD(T) calculations with an augmented triple-ζ basis set yielded essentially identical vibrational frequencies. The one exception is the torsional mode in the CH_4 + OH case, where the potential is again very flat. Altogether, these exploratory calculations for closely related systems strongly indicate that the QCISD(T)/adz method is satisfactory for the present study of the rovibrational properties of the stationary points in the CF_3H + OH system.

CF_3 + OH. The potential energy surface for the CF_3 + OH reaction has been studied with G3//B3LYP[23] calculations. Both addition−elimination and direct abstraction paths were considered in this exploration.

The addition rate constant was evaluated with variable reaction coordinate[78−80] TST employing direct CASPT2/adz evaluations of the interaction energy.[24,25] We have recently applied this direct CASPT2 VRC-TST approach to the CH_3 + OH addition reaction.[81] This study demonstrated (i) the importance of employing adz basis sets rather than dz basis sets when considering O radicals and (ii) the need to employ state averaged wave functions when considering radicals such as OH, which have degenerate orbitals.

The present study follows the procedures described in ref 81, including the incorporation of a dynamical correction factor of 0.85. However, in contrast with the CH_3 radical, the CF_3 radical is strongly nonplanar. As a result, the front and back-side additions are no longer equivalent. Indeed, preliminary calculations suggested that the contribution from the back-side addition is now negligible. Thus, the final analysis focused entirely on the front-side addition. For the OH radical, we considered only center-of-mass pivot points. For the CF_3 radicals, we again considered two sets of pivot points: a center-of-mass pivot point for large separations and a series of pivot points displaced along the C_{3v} axis for shorter separations. The Monte Carlo integrations were converged to within 5%.

All the QCISD(T), CASPT2, and MRCI calculations were performed with MOLPRO.[82] The B3LYP and G3//B3LYP calculations were performed with Gaussian 98.[83]

Discussion

The effect of CF_3 + OH, reaction 2, on the time dependence of the OH concentrations depends on both its rate coefficients and its product distribution. A schematic plot illustrating the G3//B3LYP results for the 0 K CF_3 + OH addition−elimination potential energy surface is provided in Figure 6. The initial adduct has a strong CO bond of 113.1 kcal/mol. The radical−radical nature of the CF_3O + H channel implies that there should be no reverse barrier for this channel. However, it is slightly endothermic (4.5 kcal/mol) relative to reactants. In contrast, the CF_2O + HF channel has a large reverse barrier but is highly exothermic.

There are also various abstraction channels, with that leading to CF_3H + O being exothermic by 3.4 kcal/mol. However, the saddle point for this channel lies at 9.3 kcal/mol relative to CF_3 + OH. The other abstraction channels to CF_3O + H and to CF_2 + HOF are endothermic by 4.5 and 36.6 kcal/mol, respectively. Thus, it seems unlikely that any of the abstraction channels will be significant. The large exothermicity for the CF_2O + HF products (−107.4 kcal/mol) and saddle point (−68.1 kcal/mol) implies that they should be the dominant products, with little possibility even for stabilization in the well. Thus, this channel is the one that is used in the mechanism of Table 1.

As far as we are aware, reaction 2 was first proposed by Biordi et al.;[84] however, rate constants were not determined. This reaction was mentioned as being important in later studies,[9,85] but rate constants were only estimated. Hence, the present determination for reaction 2 is apparently the first experimental determination, and an Arrhenius plot of the data is given in Figure 7, showing minimal temperature dependence within experimental error. The dynamically corrected direct CASPT2 VRC-TST predictions for reaction 2 can be represented by

$$k_{2,\mathrm{th}} = 2.42 \times 10^{-11}\, T^{-0.065} \exp(134\ K/T)\ \mathrm{cm^3\ molecule^{-1}\ s^{-1}} \quad (3)$$

Eq 3 is also plotted in Figure 7 over the present temperature range. These predictions are in remarkably good agreement with the grand average, $k_2 = (1.5 \pm 0.4) \times 10^{-11}$ cm^3 molecule^{-1} s^{-1}. The theoretical result, eq 3, suggests values ranging from 3.2 to 1.6 × 10^{-11} cm^3 molecule^{-1} s^{-1} over the temperature range 200−2000 K, respectively, indicating a slight temperature dependence. A contribution from another channel, such as the abstraction channel, might help explain the apparent rise in the experimental rate constant. However, rigid-rotor harmonic oscillator TST calculations for the lowest abstraction channel (the triplet abstraction to form CF_3H + O) yield a rate constant that is less than 5% of the addition rate constant for temperatures of 1700 K or less. Furthermore, this statement remains true even when the saddle point barrier is reduced from the G3//B3LYP

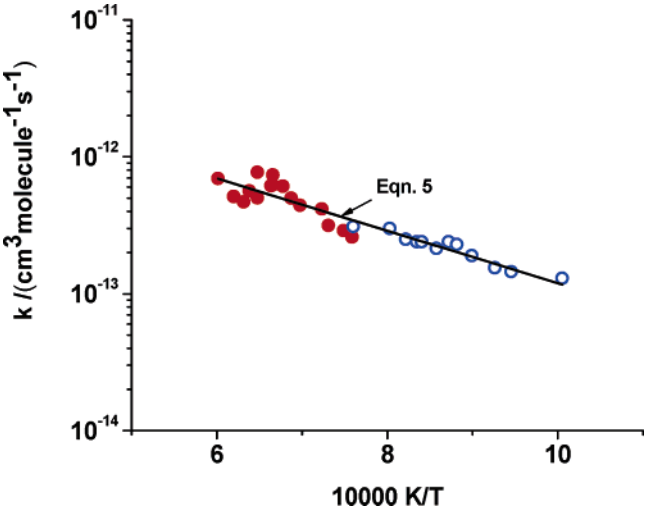

Figure 8. Arrhenius plot of the data from Table 2. Open blue circle: rate constants for k_1 (995−1316 K); red circles: rate constants for k_1 transformed from k_{-1} (1318−1663 K); and solid line: eq 5.

value by as much as 3 kcal/mol. Reductions in the barrier height by greater than 3 kcal/mol are highly unlikely.

The rate constants from Table 2 for reaction 1 between 995 and 1316 K are plotted in Arrhenius form in Figure 8. The results for reaction −1, between 1318 and 1663 K, are also tabulated in Table 2, and these can be transformed to k_1 if the equilibrium constant, $K_{-1,1} = k_{-1}/k_1$, is known. Values for $K_{-1,1}$ have been obtained from active tables[86] and fitted to a third-order polynomial form between 800 and 1600 K as

$$K_{-1,1} = (4.125 \times 10^{-12}\, T^3 - 3.29 \times 10^{-9}\, T^2 - 1.55 \times 10^{-6}\, T + 1.381 \times 10^{-3}) \quad (4)$$

Eq 4 accurately reproduces the data used to derive it within ±2.4% over the temperature range and is within 11% of the 0 K enthalpy corrected values from JANAF tables (−1,1) = 13.082 as compared to ATcT tables (−1,1) = 12.430 kcal/mol. Hence, values for $k_1 = k_{-1}/K_{-1,1}$ can be obtained from the Table 2 data, and the results are also plotted in Figure 8. Clearly, the two sets of data overlap, within experimental error and, taken together, can be described in Arrhenius form as

$$k_1 = (9.7 \pm 2.1) \times 10^{-12} \exp(-4398 \pm 275\, K/T)\ \mathrm{cm^3\ molecule^{-1}\ s^{-1}} \quad (5)$$

where the errors are at the one standard deviation level and the temperature range is 995−1663 K. The line given by eq 5 is plotted in Figure 8.

The present composite data set can then be used along with other experimental data to describe the title reaction over an extended temperature range.[87−96] Most of the lower temperature data have been obtained for use in atmospheric modeling since CF_3H is such a potent greenhouse gas. At low temperatures, there are five direct experimental rate constant studies of note, two of which are room-temperature determinations[88,89] with the other three being temperature dependent.[90−92] There are two additional temperature dependent relative rate constant studies of particular note.[93,94] Prior to the present study, there are two high-temperature determinations, one at 1350 K by Ernst et al. who report $k_1 = 6.64 \times 10^{-13}$ cm^3 molecule^{-1} s^{-1},[95] and the other being a relative study by Bradley et al.[96] Three of the single temperature determinations[88,89,95] are plotted along with the present data in Figure 9. Using the Arrhenius equations that

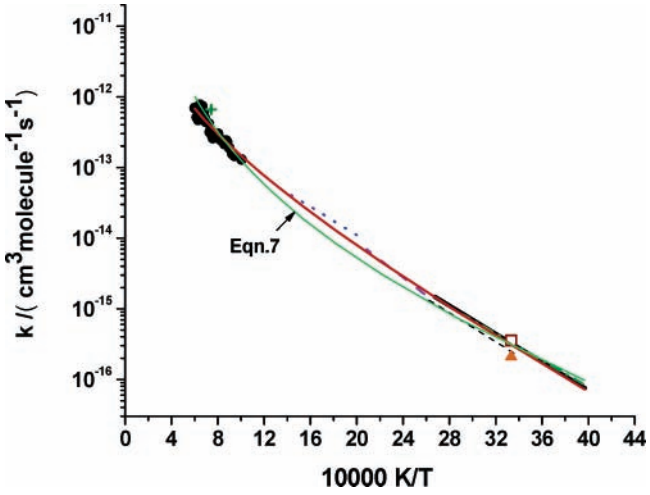

Figure 9. Comparison of the present work with recent experimental results for k_1. ●: Present work (995−1663 K), solid line over the entire temperature range (252−1663 K); eq 6 evaluation in text. Green cross: ref 95, dotted line: ref 92, thick dashed line: ref 90, thin dashed line: ref 93, thick solid line: ref 91, dashed−dotted line: ref 94, red open square: ref 89, and red triangle:− ref 88. Also shown is the theoretical result of eq 7 in text.

describe the results from the five temperature dependent studies,[90−94] a database, over equal intervals of T^{-1}, has been constructed. Six points from each of the five temperature dependent studies are calculated from the equations but only over the temperature range of the individual studies. The single points from Howard and Evenson,[88] Nip et al.,[89] and Ernst et al.[95] are also included. The 28 points from the present study (see Table 2) complete the database. Hence, these 61 points constitute the database for determining an evaluation from 252 to 1663 K. The database is then fitted to the modified three parameter Arrhenius equation, $k = AT^n \exp(-B/T)$, yielding

$$k_1 = 2.08 \times 10^{-17}\, T^{1.5513} \exp(-1848\, K/T)\ \mathrm{cm^3\ molecule^{-1}\ s^{-1}} \quad (6)$$

The largest experimental deviation from eq 6 (75% higher) is the result of Ernst et al.,[95] with all other values agreeing within combined experimental errors. The results of Schmoltner et al.[91] are uniformly 5% higher, those of Medhurst et al.[92] being 0−40% higher, those of Jeong and Kaufman[90] being within ±10%, those of Hsu and DeMore[93] being 18% lower, and those of Chen et al.[94] being 2−16% higher. The room-temperature value of Nip et al.[89] is 17% higher, whereas that of Howard and Evenson[88] is 31% lower. The points from the present determination are within ±18% (at the one standard deviation level) of the line determined from eq 6. Hence, the evaluation is an excellent representation of the present and previous determinations on the title reaction. This is illustrated graphically in Figure 9 where the lines specified from these earlier studies are shown over the individual experimental temperature ranges along with the line describing the eq 6 evaluation.

There are three pertinent earlier theoretical investigations on reactions 1 and −1[19−21] of varying degrees of complexity. Pasteris et al.[19] used the bond energy-bond order (BEBO) method to estimate barrier heights, force fields, and configurations to calculate rate constant values for k_{-1}. Their results on transformation to k_1 give predictions that are high by ∼10. Fu et al.[20] used QCISD/6-311G**//MP2/6-311G** ab initio calculations along with transition state theory (TST) to estimate rate constants between 200 and 500 K. These results are about

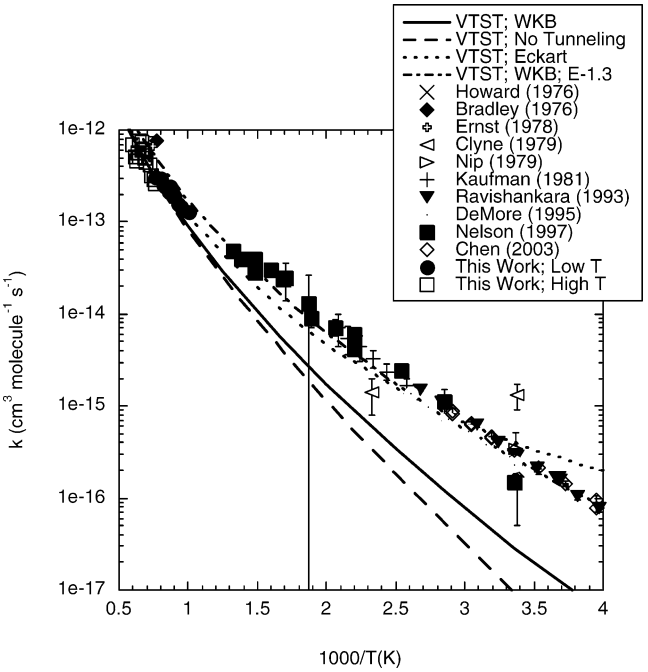

Figure 10. Plot of the temperature dependence of the rate constant for the CF_3H + OH reaction. The solid line denotes the present VTST calculations employing WKB estimates for the tunneling through the vibrationally adiabatic ground (VAG) state potential. The long dashed line denotes calculations that neglect tunneling. The dotted line denotes calculations where the WKB−VAG transmission coefficients are replaced with asymmetric Eckart tunneling probabilities. The dashed−dotted lines show the effect of decreasing the saddle point energy by 1.3 kcal/mol.

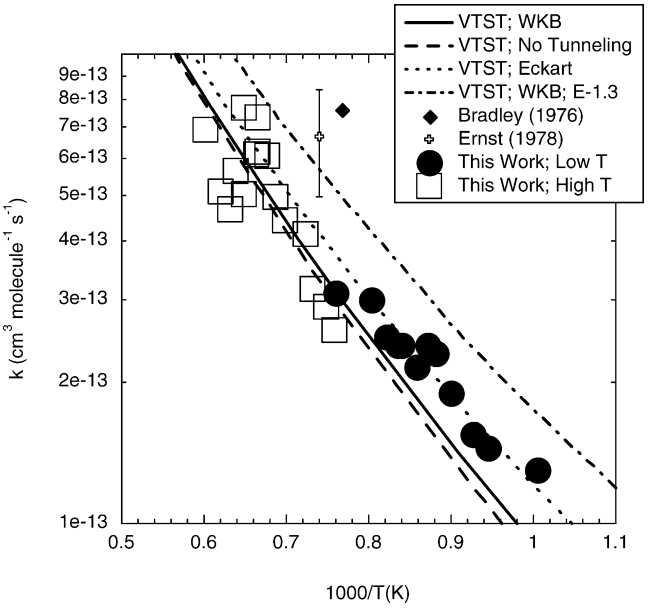

Figure 11. Plot of the temperature dependence of the rate constant for the CF_3H + OH reaction in the high-temperature regime. Lines and symbols are as in Figure 10.

a factor of 3 lower than values from eq 6. Last, Schwartz et al.[21] also used ab initio theory to estimate configurations and force fields. They did calculations on the OH + CH_xF_y → $CH_{x-1}F_y$ + H_2O reactions using TST with Eckart tunneling factors derived from the ab initio results for the transition states. They then modified the method used for tunneling for all cases and obtained much better agreement with experiment for four reactions, OH + CH_4, CH_3F, CH_2F_2, and CHF_3. Their predictions at low temperatures are in excellent agreement with eq 6 but then start to diverge at $T > \sim 500$ K, becoming 6 times larger at $T = 1700$ K.

The present theoretical predictions for the temperature dependence of the CF_3H + OH abstraction rate constant are illustrated in Figures 10 and 11. The full temperature range is considered in Figure 10, while Figure 11 emphasizes the range corresponding to the present experimental study. The primary theoretical result (solid line), corresponding to the VTST calculations with WKB estimates for tunneling through the vibrationally adiabatic ground state potential, is in quantitative agreement with the present experimental measurements. However, at lower temperatures, these theoretical predictions significantly underestimate the rate constant. At 300 K, they are a factor of 10 too low.

This underestimate may be an indication that either the calculated barrier is too high or we are underestimating the extent of tunneling. Lowering the zero-point corrected saddle point by 1.3 kcal/mol from its QCISD(T)/CBS//QCISD(T)/adz calculated value of 6.33 kcal/mol yields the dashed−dotted curve, which is in quantitative agreement with the low-temperature experimental results but overestimates the present experimental results by about a factor of 1.4. This level of agreement for such a broad temperature range is quite remarkable. Furthermore, an error of this magnitude in the ab initio predictions for the barrier height is within the general uncertainty limits for calculations at this level of theory. However, the high accuracy of such ab initio predictions for the H_2 + OH and CH_4 + OH reactions, where the errors appear to be less than 0.2 kcal/mol (and in opposite direction), argues against an error as large as 1.3 kcal/mol.

The accurate prediction of tunneling probabilities is an inherently difficult task. The WKB evaluation of the tunneling through vibrationally adiabatic barriers is a fundamentally more meaningful approach than the more standard asymmetric Eckart evaluations. However, for the present reaction, the asymmetric Eckart approach (dotted line in Figures 10 and 11) yields a much improved agreement with the low-temperature experimental data, due to its higher second derivative for the reactive mode of the potential. This higher second derivative for the Eckart case is not correct, but it does have the effect of increasing the tunneling probability, just as would the consideration of alternative corner cutting tunneling paths. Thus, the improved agreement is to some degree the result of a fortunate cancellation of errors.

Alternatively, the experimental data may be fitted by adjusting both the saddle point energy and the tunneling probability. For example, we have decreased the barrier height by 0.6 kcal/mol, while simultaneously employing an asymmetric Eckart potential but with an imaginary frequency of 1500 cm^{-1}. The resulting rate constants agree with the evaluation provided by eq 6 to within a factor of 1.6 over the range of that evaluation (252−1663 K). For temperatures 250−2250 K, this empirical result fits the expression

$$k_{1,\mathrm{th}} = 1.78 \times 10^{-23}\, T^{3.406} \exp(-837\, K/T)\ \mathrm{cm^3\ molecule^{-1}\ s^{-1}} \quad (7)$$

to within 15%. This result has no particular value for temperatures in the range of applicability of eq 6 but does serve the purpose of providing a meaningful extrapolation to higher temperatures.

Finally, we note that the displacement of the barrier maximum from the electronic maximum to the zero-point corrected

maximum has a modest effect on the rate constant prediction, decreasing it by a factor of 0.65 at 250 K. By 2250 K, this reduction factor is 0.9. Meanwhile, variational effects from the zero-point corrected barrier are minimal, reducing the rate by less than 10% for the 250−2250 K temperature range. The smallness of this variational correction is fairly typical for reactions such as this, which have a sharp well-defined barrier. However, the anharmonicity factor decreases from 0.86 at 250 K to 0.62 at 2250 K. These values are considerably closer to unity than Seta et al.[67] found in their treatment of the OH + benzene reaction but are likely quite similar to the values they obtained for the OH + toluene reaction.

Acknowledgment. This work was supported by the U.S. Department of Energy, Office of Basic Energy, Sciences Division of Chemical Sciences, Geosciences, and Biosciences under Contract DE-AC02-06CH11357.

Supporting Information Available: Geometries and vibrational frequencies from both the B3LYP/6-311++G(d,p) and QCISD(T)/adz evaluations for the reactants, transition state, and products in the CF3H + OH reaction. This material is available free of charge via the Internet at http://pubs.acs.org.

References and Notes

(1) Babushok, V.; Burgess, D. R. F.; Miziolek, A.; Tsang, W. In *Halon Replacements: Technology and Science*; Miziolek, A., Tsang, W., Eds.; American Chemical Society: Washington, DC, 1995; Vol. 611, p 275.

(2) Andersen, S. O.; Metchis, K. L.; Rubenstein, R. In *Halon Replacements: Technology and Science*; Miziolek, A., Tsang, W., Eds.; American Chemical Society: Washington, DC, 1995; Vol. 611, p 8.

(3) Babushok, V.; Noto, T.; Burgess, D. R. F.; Hamins, A.; Tsang, W. *Combust. Flame* **1996**, *107*, 351.

(4) Berry, R. J.; Burgess, D. R. F., Jr.; Nyden, M. R.; Zachariah, M. R.; Schwartz, M. *J. Phys. Chem.* **1995**, *99*, 17145.

(5) Linteris, G. T.; Burgess, D. R. F., Jr.; Babushok, V.; Zachariah, M.; Tsang, W.; Wesmoreland, P. *Combust. Flame* **1998**, *113*, 164.

(6) Westbrook, C. K. *Combust. Sci. Technol.* **1983**, *34*, 201.

(7) Sanogo, O.; Delfau, J. L.; Akrich, R.; Vovelle, C. *Proc. Combust. Inst.* **1995**, *25*, 1489.

(8) Vovelle, C.; Delfau, J.-L.; Sanofo, O. In *Final Report in the EC Environment Program "Substitutes for Halons (SUBSTHAL)" EV5V-CT92-0230*; Battin-Leclerc, F., Come, G. M., Baronnet, F., Eds.; 1995; p 74.

(9) Battin-Leclerc, F.; Smith, A. P.; Hayman, G. D.; Murrells, T. P. *J. Chem. Soc., Fraraday Trans.* **1996**, *92*, 3305.

(10) *NIST Chemical Kinetics Database*; NIST Standard Reference Database 17: Gaithersburg, MD, 2000.

(11) Kiefer, J. H.; Sathyanarayana, R.; Lim, K. P.; Michael, J. V. *J. Phys. Chem.* **1994**, *98*, 12278.

(12) Kumaran, S. S.; Su, M.-C.; Lim, K. P.; Michael, J. V. *Chem. Phys. Lett.* **1995**, *243*, 59.

(13) Hranisavljevic, J.; Carroll, J. J.; Su, M.-C.; Michael, J. V. *Int. J. Chem. Kinet.* **1998**, *30*, 859.

(14) Hranisavljevic, J.; Michael, J. V. *J. Phys. Chem.* **1998**, *102*, 7668.

(15) Su, M.-C.; Kumaran, S. S.; Lim, K. P.; Michael, J. V. *Rev. Sci. Instrum.* **1995**, *66*, 4649.

(16) Su, M.-C.; Kumaran, S. S.; Lim, K. P.; Michael, J. V.; Wagner, A. F.; Harding, L. B.; Fang, D.-C. *J. Phys. Chem. A* **2002**, *106*, 8261.

(17) Srinivasan, N. K.; Su, M.-C.; Sutherland, J. W.; Michael, J. V. *J. Phys. Chem. A* **2005**, *109*, 1857.

(18) Srinivasan, N. K.; Su, M.-C.; Sutherland, J. W.; Michael, J. V. *J. Phys. Chem. A* **2005**, *109*, 7902.

(19) Pasteris, L.; Oexler, E. V.; Staricco, E. H. *Int. J. Chem. Kinet.* **1983**, *15*, 835.

(20) Fu, Y.; Lewis-Bevan, W.; Tyrrell, J. *J. Phys. Chem.* **1995**, *99*, 630.

(21) Schwartz, M.; Marshall, P.; Berry, R. J.; Ehlers, C. J.; Petersson, G. A. *J. Phys. Chem. A* **1998**, *102*, 10074.

(22) El-Taher, S. *Int. J. Quantum Chem.* **2001**, *84*, 426.

(23) Baboul, A. G.; Curtiss, L. A.; Redfern, P. C.; Rahavachari, K. *J. Chem. Phys.* **1999**, *110*, 7650.

(24) Harding, L. B.; Georgievskii, Y.; Klippenstein, S. J. *J. Phys. Chem. A* **2005**, *109*, 4646.

(25) Klippenstein, S. J.; Georgievskii, Y.; Harding, L. B. *Phys. Chem. Chem. Phys.* **2006**, *10*, 1133.

(26) Michael, J. V. *Prog. Energy Combust. Sci.* **1992**, *18*, 327.

(27) Michael, J. V. In *Advances in Chemical Kinetics and Dynamics*; Barker, J. R., Ed.; JAI: Greenwich, 1992; Vol. 1, pp 47−112.

(28) Michael, J. V.; Sutherland, J. W. *Int. J. Chem. Kinet.* **1986**, *18*, 409.

(29) Michael, J. V. *J. Chem. Phys.* **1989**, *90*, 189.

(30) Michael, J. V.; Fisher, J. R. In *Seventeenth International Symposium on Shock Waves and Shock Tubes*; Kim, Y. W., Ed.; AIP Conference Proceedings 208, American Institute of Physics: New York, 1990; pp 210−215.

(31) Su, M.-C.; Kumaran, S. S.; Lim, K. P.; Michael, J. V.; Wagner, A. F.; Dixon, D. A.; Kiefer, J. H.; DiFelice, J. *J. Phys. Chem.* **1996**, *100*, 15827.

(32) Du, H.; Hessler, J. P. *J. Chem. Phys.* **1992**, *96*, 1077.

(33) Ruscic, B.; Wagner, A. F.; Harding, L. B.; Asher, R. L.; Feller, D.; Dixon, D. A.; Peterson, K. A.; Song, Y.; Qian, X.; Ng, C. Y.; Liu, J.; Chen, W.; Schwenke, D. W. *J. Phys. Chem. A* **2002**, *106*, 2727.

(34) Herbon, J. T.; Hanson, R. K.; Golden, D. M.; Bowman, C. T. *Proc. Combust. Inst.* **2002**, *29*, 1201.

(35) Oldenborg, R. C.; Loge, G. W.; Harridine, D. M.; Winn, K. R. *J. Phys. Chem.* **1992**, *96*, 8426.

(36) Wooldridge, M. S.; Hanson, R. K.; Bowman, C. T. *Int. J. Chem. Kinet.* **1994**, *26*, 389.

(37) Krasnoperov, L. N.; Chesnokov, E. N.; Stark, H.; Ravishankara, A. R. *J. Phys. Chem. A* **2004**, *108*, 11526.

(38) Michael, J. V.; Su, M.-C.; Sutherland, J. W.; Carroll, J. J.; Wagner, A. F. *J. Phys. Chem. A* **2002**, *106*, 5297.

(39) Baulch, D. L.; Cobos, C. J.; Cox, R. A.; Esser, C.; Frank, P.; Just, Th.; Kerr, J. A.; Pilling, M. J.; Troe, J.; Walker, R. W.; Warnatz, J. *J. Phys. Chem. Ref. Data* **1992**, *21*, 411.

(40) Michael, J. V.; Kumaran, S. S.; Su, M.-C. *J. Phys. Chem. A* **1999**, *103*, 5942.

(41) Srinivasan, N. K.; Su, M.-C.; Sutherland, J. W.; Michael, J. V. *J. Phys. Chem. A* **2005**, *109*, 7902.

(42) Lim, K. P.; Michael, J. V. *Proc. Combust. Inst.* **1994**, *25*, 713.

(43) Lim, K. P.; Michael, J. V. *J. Chem. Phys.* **1993**, *98*, 3919.

(44) (a) Fockenberg, C.; Hall, G. E.; Preses, J. M.; Sears, T. J.; Muckerman, J. T. *J. Phys. Chem. A* **1999**, *103*, 5722. (b) Preses, J. M.; Fockenberg, C.; Flynn, G. W. *J. Phys. Chem. A* **2000**, *104*, 6758.

(45) Srinivasan, N. K.; Su, M.-C.; Michael, J. V. *J. Phys. Chem. A* **2007**, *111*, 3951.

(46) Michael, J. V.; Keil, D. G.; Klemm, R. B. *Int. J. Chem. Kinet.* **1985**, *15*, 705.

(47) Tully, F. P. *Chem. Phys. Lett.* **1988**, *143*, 510.

(48) Langford, A. O.; Petek, H.; Moore, C. B. *J. Chem. Phys.* **1983**, *78*, 6650.

(49) Hancock, G.; Heal, M. R. *J. Phys. Chem.* **1992**, *96*, 10316.

(50) Jasper, A. W.; Klippenstein, S. J.; Harding, L. B. Personal communication, October 2006.

(51) Gonzalez, C.; Theisen, J.; Schlegel, H. B.; Hase, W. L.; Kaiser, E. W. *J. Phys. Chem.* **1992**, *96*, 1767.

(52) Vasudevan, V.; Davidson, D. F.; Hanson, R. K. *Int. J. Chem. Kinet.* **2005**, *37*, 98.

(53) Fernandez, A.; Fontijn, A. *J. Phys. Chem. A* **2001**, *105*, 8196.

(54) Jasper, A. W.; Klippenstein, S. J. Personal communication, October 2006.

(55) Schug, K. P.; Wagner, H. Gg.; Zabel, F. *Ber. Bunsen. Phys. Chem.* **1979**, *83*, 167.

(56) Stevens, P. S.; Brune, W. H.; Anderson, J. G. *J. Phys. Chem.* **1989**, *93*, 4068.

(57) Vasudevan, V.; Davidson, D. F.; Hanson, R. K. *J. Phys. Chem. A* **2005**, *109*, 3352.

(58) Krasnoperov, L. N.; Michael, J. V. *J. Phys. Chem. A* **2004**, *108*, 5643.

(59) Pople, J. A.; Head-Gordon, M.; Raghavachari, K. *J. Chem. Phys.* **1987**, *87*, 5968.

(60) Dunning, T. H., Jr. *J. Chem. Phys.* **1989**, *90*, 1007.

(61) Feller, D.; Dixon, D. A. *J. Chem. Phys.* **2001**, *115*, 3484.

(62) Martin, J. M. L. *Chem. Phys. Lett.* **1996**, *259*, 669.

(63) Greenwald, E. E.; North, S. W.; Georgievskii, Y.; Klippenstein, S. J. *J. Phys. Chem. A* **2005**, *109*, 6031.

(64) Becke, A. D. *J. Chem. Phys.* **1993**, *98*, 5648.

(65) Hehre, W. J.; Radom, L.; Pople, J. A.; Schleyer, P. v. R. *Ab Initio Molecular Orbital Theory*; Wiley: New York, 1987.

(66) Srinivasan, N. K.; Michael, J. V.; Harding, L. B.; Klippenstein, S. J. *Combust. Flame* **2007**, *149*, 104.

(67) Seta, T.; Nakajima, M.; Miyoshi, A. *J. Phys. Chem. A* **2006**, *110*, 5081.

(68) Garrett, B. C.; Truhlar, D. G. *J. Phys. Chem.* **1979**, *83*, 2921.

(69) Marcus, R. A.; Coltrin, M. E. *J. Chem. Phys.* **1977**, *67*, 2609.

(70) Truong, T. N.; Lu, D.-h.; Lynch, G. C.; Liu, Y.-P.; Melissas, V. S.; Stewart, J. J.; Steckler, R.; Garrett, B. C.; Isaacson, A. D.; Gonzalez-Lafont, A.; Rai, S. N.; Hancock, G. C.; Joseph, T.; Truhlar, D. G. *Comput. Phys. Commun.* **1993**, *75*, 143.

(71) Liu, Y.-P.; Lynch, G. C.; Truong, T. N.; Lu, D.-h.; Gonzalez-Lafont, A.; Truhlar, D. G.; Garrett, B. C. *J. Am. Chem. Soc.* **1993**, *115*, 7806.
(72) Truhlar, D. G.; Garrett, B. C.; Klippenstein, S. J. *J. Phys. Chem.* **1996**, *100*, 12771.
(73) Lee, T. J.; Taylor, P. R. *Int. J. Quant. Chem.* **1989**, *23*, 199.
(74) Lee, T. J.; Rendell, A. P.; Taylor, P. R. *J. Phys. Chem.* **1990**, *94*, 5463.
(75) (a) Langhoff, S. R.; Davidson, E. R. *Int. J. Quantum Chem.* **1974**, *8*, 61. (b) Silver, D. W.; Davidson, E. R. *Chem. Phys. Lett.* **1978**, *52*, 403.
(76) Yang, M.; Zhang, D. H.; Collins, M. A.; Lee, S.-Y. *J. Chem. Phys.* **2001**, *114*, 4759.
(77) Espinosa-Garcia, J.; Corchado, J. C. *J. Chem. Phys.* **2000**, *112*, 5731.
(78) Klippenstein, S. J. *J. Chem. Phys.* **1992**, *96*, 367.
(79) Klippenstein, S. J. *J. Phys. Chem.* **1994**, *98*, 11459.
(80) Georgievskii, Y.; Klippenstein, S. J. *J. Chem. Phys.* **2003**, *118*, 5442.
(81) Jasper, A. W.; Klippenstein, S. J.; Harding, L. B.; Ruscic, B. *J. Phys. Chem. A* **2007**, *111*, 3932.
(82) MOLPRO, version 2002.1, is a package of ab initio programs written by Werner, H.-J. and Knowles, P. J. with contributions from Amos, R. D.; Bernhardsson, A.; Berning, A.; Celani, P.; Cooper, D. L.; Deegan, M. J. O.; Dobbyn, A. J.; Eckert, F.; Hampel, C.; Hetzer, G.; Korona, T.; Lindh, R.; Lloyd, A. W.; McNicholas, S. J.; Manby, F. R.; Meyer, W.; Mura, M. E.; Nicklaâ, A.; Palmieri, P.; Pitzer, R.; Rauhut, G.; Schütz, M.; Schumann, U.; Stoll, H.; Stone A. J.; Tarroni, R.; Thorsteinsson, T.; Werner, H.-J.
(83) Frisch, M. J.; Trucks, G. W.; Schlegel, H. B.; Scuseria, G. E.; Robb, M. A.; Cheeseman, J. R.; Zakrzewski, V. G.; Montgomery, J. A., Jr.; Stratmann, R. E.; Burant, J. C.; Dapprich, S.; Millam, J. M.; Daniels, A. D.; Kudin, K. N.; Strain, M. C.; Farkas, O.; Tomasi, J.; Barone, V.; Cossi, M.; Cammi, R.; Mennucci, B.; Pomelli, C.; Adamo, C.; Clifford, S.; Ochterski, J.; Petersson, G. A.; Ayala, P. Y.; Cui, Q.; Morokuma, K.; Salvador, P.; Dannenberg, J. J.; Malick, D. K.; Rabuck, A. D.; Raghavachari, K.; Foresman, J. B.; Cioslowski, J.; Ortiz, J. V.; Baboul, A. G.; Stefanov, B. B.; Liu, G.; Liashenko, A.; Piskorz, P.; Komaromi, I.; Gomperts, R.; Martin, R. L.; Fox, D. J.; Keith, T.; Al-Laham, M. A.; Peng, C. Y.; Nanayakkara, A.; Challacombe, M.; Gill, P. M. W.; Johnson, B.; Chen, W.; Wong, M. W.; Andres, J. L.; Gonzalez, C.; Head-Gordon, M.; Replogle, E. S.; Pople, J. A. *Gaussian 98*, revision A.11; Gaussian, Inc.: Pittsburgh, PA, 2001.
(84) Biordi, J. C.; Lazzara, C. P.; Popp, J. F. *J. Phys. Chem.* **1978**, *82*, 125.
(85) Richter, H.; Vandooren, J.; Van Tiggelen, P. J. *Proc. Combust. Inst.* **1994**, *25*, 825.
(86) Ruscic, B. Personal communication of unpublished results obtained from Active Thermochemical Tables 1.25 and the Core (Argonne) Thermochemical Network 1.049 (2005) Tables.
(87) Clyne, M. A. A.; Holt, P. M. *J. Chem. Soc., Faraday Trans. 2* **1979**, *75*, 582.
(88) Howard, C. J.; Evenson, K. M. *J. Chem. Phys.* **1976**, *64*, 197.
(89) Nip, W. S.; Singleton, D. L.; Overend. R.; Paraskevopoulos, G. *J. Phys. Chem.* **1979**, *83*, 2240.
(90) Jeong, K.-M.; Kaufman, F. *J. Phys. Chem.* **1982**, *86*, 1808.
(91) Schmoltner, A. M.; Talukdar, R. K.; Warren, R. F.; Mellouki, A.; Goldfarb, L.; Gierczak, T.; McKeen, S. A.; Ravishankara, A. R. *J. Phys. Chem.* **1993**, *97*, 8976.
(92) Medhurst, L. J.; Fleming, J.; Nelson, H. H. *Chem. Phys. Lett.* **1997**, *266*, 607.
(93) Hsu, K.-J.; DeMore, W. B. *J. Phys. Chem.* **1995**, *99*, 1235.
(94) Chen, L.; Kutsuna, S.; Tokuhashi, K.; Sekiya, A. *Int. J. Chem. Kinet.* **2003**, *35*, 317.
(95) Ernst, J.; Wagner, H. Gg.; Zellner, R. *Ber. Bunsen. Phys. Chem.* **1978**, *82*, 409.
(96) Bradley, J. N.; Capey, W. D.; Fair, R. W.; Pritchard, D. K. *Int. J. Chem. Kinet.* **1976**, *8*, 549.